turbance, viscous and Coulomb friction, the proposed control scheme displays a very high capacity of precision control.

V. CONCLUSION

A novel tracking controller with an NN that incorporates a knowledge base has been proposed for servo systems, which is robust to structured as well as unstructured uncertainties. Since a staggered control strategy is employed, the influences from plant variation and measurement noise, etc., would not have an undesirable effect on the tracking performance. The high speed of response and the ability at which it could control a highly nonlinear system without the necessity of having *a priori* knowledge of the servo system is a major advantage of this control scheme. Further input parameters, such as the acceleration, could also be incorporated easily to enhance the performance of the system.

REFERENCES

[1] H. Hashimoto, K. Maruyama, and F. Harashima, "A microprocessor-based robot manipulator control with sliding mode," *IEEE Trans. Ind. Electron.*, vol. 34, pp. 11–18, Feb. 1987.
[2] M. El-Sharkawi and C. Huang, "Variable structure tracking of D.C. motor for high performance applications," *IEEE Trans. Energy Conversion*, vol. 4, pp. 643–650, Dec. 1989.
[3] G. Niemeyer and J. J. E. Slotine, "Performance in adaptive control of robotic manipulators," *Int. J. Robot. Res.*, vol. 10, no. 2, pp. 149–161, 1991.
[4] L. A. Dessaint, M. Saad, B. Hebert, and K. Al-Haddad, "An adaptive controller for a direct-drive SCARA robot," *IEEE Trans. Ind. Electron.*, vol. 39, pp. 105–111, Apr. 1992.
[5] M. J. Er and K. C. Liew, "Control of adept SCARA robot using neural networks," *IEEE Trans. Ind. Electron.*, vol. 44, pp. 762–768, Dec. 1997.
[6] S. S. Ge, C. C. Hang, and L. C. Woon, "Adaptive neural network control of robot manipulators in task space," *IEEE Trans. Ind. Electron.*, vol. 44, pp. 746–752, Dec. 1997.

Envelope Simulation by SPICE-Compatible Models of Electric Circuits Driven by Modulated Signals

Sam Ben-Yaakov, Stanislav Glozman, and Raul Rabinovici

Abstract—SPICE-compatible equivalent circuits were developed to facilitate the analysis and envelope simulation of electric circuits driven by modulated signals. The circuits are based on a novel complex phasor domain transformation. The proposed method facilitates fast simulation of any general linear circuit driven by a modulated signal, such as amplitude, frequency, or phase modulation.

Index Terms—Envelope detection, modeling, simulation, SPICE.

I. INTRODUCTION

Modulated signals play an important role in power electronics. For example, frequency or phase modulation (FM, PM) is related to resonant power converters [1] and to electronic ballasts of discharge lamps

[2]. Furthermore, amplitude modulation (AM) plays an important role in determining the stability of high-frequency electronic ballasts for discharge lamps [3], [4]. In these systems, the lamp is driven by a high-frequency source in series with an inductor which controls the current. Power level is normally regulated by shifting the frequency of the source and, thereby, increasing or decreasing the current. Hence, current level can be closely controlled by a feedback network connected to a controlled oscillator that feeds the power stage. It should be noted that when the FM signal passes through reactive elements it would be translated to an amplitude modulated (AM) FM signal. Direct analysis of the response of such an electrical circuit to a modulated carrier is, thus, complex, while cycle-by-cycle simulation of such a system is very lengthy due to the presence of the high-frequency component.

In this letter, we developed a complex phasor transformation approach that was then used to derive a SPICE-compatible model transparent to the high-frequency carrier. The proposed method facilitates envelope simulation of any linear electric circuit by any general purpose simulator. This approach differs from earlier solutions to envelope simulation, which rely on specialized computer programs [5].

II. COMPLEX PHASOR TRANSFORMATION APPROACH

Any analog modulated signal (AM, FM, or PM) can be described by the following general expression:

$$u(t) = U_1(t) \cdot \cos \omega_c t + U_2(t) \cdot \sin \omega_c t \qquad (1)$$

where $U_1(t)$ and $U_2(t)$ are the components of the modulation signal and ω_c is the angular frequency of the carrier.

Expression (1) could also be written as

$$u(t) = \mathrm{Re}[(U_1(t) - j \cdot U_2(t)) \cdot \exp(j\omega_c t)] \qquad (2)$$

or as

$$u(t) = |U(t)| \cdot \mathrm{Re}[\exp(\arg(U(t))) \cdot \exp(j\omega_c t)] \qquad (3)$$

where "$\arg(U(t))$" is $\tan^{-1}((-U_2(t))/(U_1(t)))$.

Expression (3) implies that the modulated signal in the time domain $u(t)$ can be represented by a generalized phasor that both its magnitude and phase are time dependent. The expression of the complex phasor $\vec{U}(t)$ is

$$\vec{U}(t) = U_1(t) - jU_2(t). \qquad (4)$$

The magnitude

$$|\vec{U}(t)| = [U_1^2(t) + U_2^2(t)]^{1/2} \qquad (5)$$

is equal to the modulation envelope of the original signal $u(t)$ in (3).

As will be shown next, the complex phasor representation $\vec{U}(t) = U_1(t) - jU_2(t)$ introduced here can be used to drive the low-frequency equivalent circuits that represent the envelope behavior of the system without involving the high-frequency carrier.

III. GENERAL CASE

Consider a general R–L–C circuit that is driven by a modulated carrier $u(t)$. The matrix state-space equation of the system is

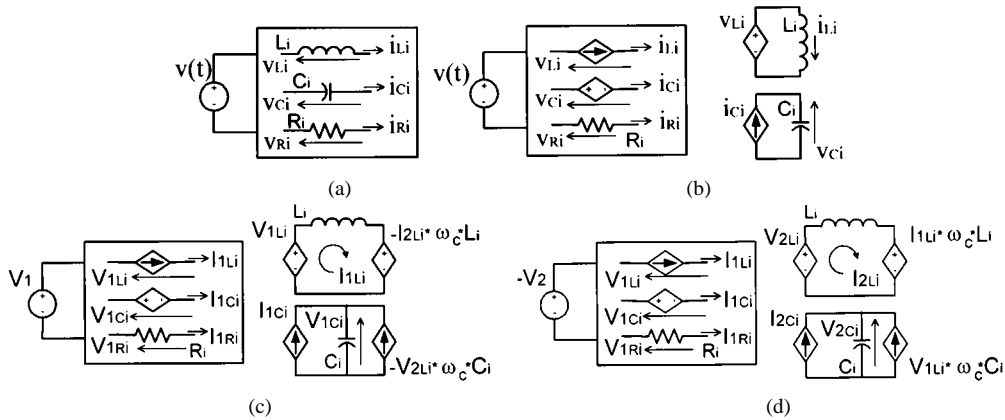$$\dot{x} = A \cdot x + B \cdot u. \qquad (6)$$

Fig. 1. Derivation of phasor equivalent circuits. (a) Original circuit. (b) Replacing reactive elements by dependent sources. (c) Real part of phasor equivalent circuit. (d) Imaginary part of phasor equivalent circuit.

By expressing u as the complex excitation (4), inserting it in (6), and breaking the resulting complex state-space equation into real and imaginary parts one obtains

$$\dot{X}_1 = A \cdot X_1 - A_1 \cdot X_2 + B \cdot U_1 \qquad (7)$$

$$\dot{X}_2 = A \cdot X_2 + A_1 \cdot X_1 - B \cdot U_2 \qquad (8)$$

where X_1, X_2 are the complex state variables of the phasor domain circuit, U_1, U_2 are the source complex phasor components, and A_1 is the matrix of the imaginary resistors [6], $j\omega_c L$ associated with each inductor and $1/j\omega_c C$ associated with each capacitor (ω_c is the carrier frequency [6]). The cross-coupled terms $A_1 X_2$ in (7) and $A_1 X_1$ in (8) can be represented as dependent sources: voltage source in the inductor case and current source for the capacitor case. Original resistors are left as is. Equations (7) and (8) can now be simulated as two circuits that include dependent sources that are a function of the state variables of the cross circuits. Note that (7) and (8) include only the low-frequency component, while the high-frequency carrier is present only as an algebraic coefficient (ω_c).

IV. IMPLEMENTATION

Preparation of (7) and (8) for analysis by a general purpose analog circuit simulator can proceed by translating the equations into equivalent circuits. Matrix "A" is that of the original circuit, whereas "'A_1'" is a new matrix representing the coupled dependent sources. Here, we describe a direct method that bypasses the need for constructing the new matrix. Starting with a general R–L–C circuit [Fig. 1(a)] that is driven by a modulated carrier $v(t)$, we first replace the reactive elements by dependent sources. An inductor L_i is replaced by a current source i_{Li} and a capacitor C_i is replaced by a voltage source v_{Ci} [Fig. 1(b)]. The magnitude of the dependent sources is linked to auxiliary circuits that emulate the behavior of the elements. That is, the auxiliary circuit for L_i comprises a dependent voltage source v_{Li} that forces the in-circuit voltage on the inductor L_i. The current generated in the auxiliary circuit is then fed back to the main circuit by the dependent current source i_{Li} that represents the inductor. In a similar way, dependent voltage sources v_{Ci} replace capacitors in the main circuit. This separation step is not crucial, but is used to streamline the structure of the equivalent circuits that will later evolve.

The next step applies the transformation of the circuit into two phasor circuits per (7) and (8). Now, we apply the two phasor sources V_1 and
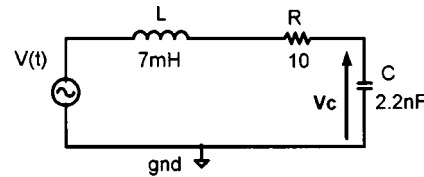

Fig. 2. Illustrative circuit.

$-V_2$ and implement the dependent sources $A_1 X_2$ and $A_1 X_1$. These are shown schematically in Fig. 1(c) (real part) and Fig. 1(d) (imaginary part) for a specific inductor L_i and a capacitor C_i.

The state equations that represent an original inductor L_i [Fig. 1(a)] are, thus, for the real part [Fig. 1(c)]

$$L_i \cdot \frac{dI_{1Li}}{dt} = V_{1Li} + I_{2Li} \cdot \omega_c \cdot L_i \qquad (9)$$

and for the imaginary part [Fig. 1(d)]

$$L_i \cdot \frac{dI_{2Li}}{dt} = V_{2Li} - I_{1Li} \cdot \omega_c \cdot L_i. \qquad (10)$$

The state equations that represent an original capacitor C_i [Fig. 1(a)] are for the real part [Fig. 1(c)]

$$C_i \cdot \frac{dV_{1Ci}}{dt} = I_{1Ci} + V_{2Ci} \cdot \omega_c \cdot C_i \qquad (11)$$

and for the imaginary part [Fig. 1(d)]

$$C_i \cdot \frac{dV_{2Ci}}{dt} = I_{2Ci} - V_{1Ci} \cdot \omega_c \cdot C_i. \qquad (12)$$

The equivalent circuits of Fig. 1(c) and (d) are now SPICE compatible. They include the original R–L–C components and dependent sources. It should be noted that the dependent sources are a function of the signals in the cross circuits. That is, the dependent sources in the real section [$-I_{2Li} \cdot \omega_c \cdot L_i$, $-V_{2Ci} \cdot \omega_c \cdot C_i$, Fig. 1(c)] depend on the corresponding signals in the imaginary part [Fig. 1(d)] and vice versa.

The circuits of Fig. 1(c) and (d) are compatible with any modern circuit simulator. In the following, we present an example that was run on PSPICE (MicroSim Inc., Evaluation Version 8), but any other simulator will do.
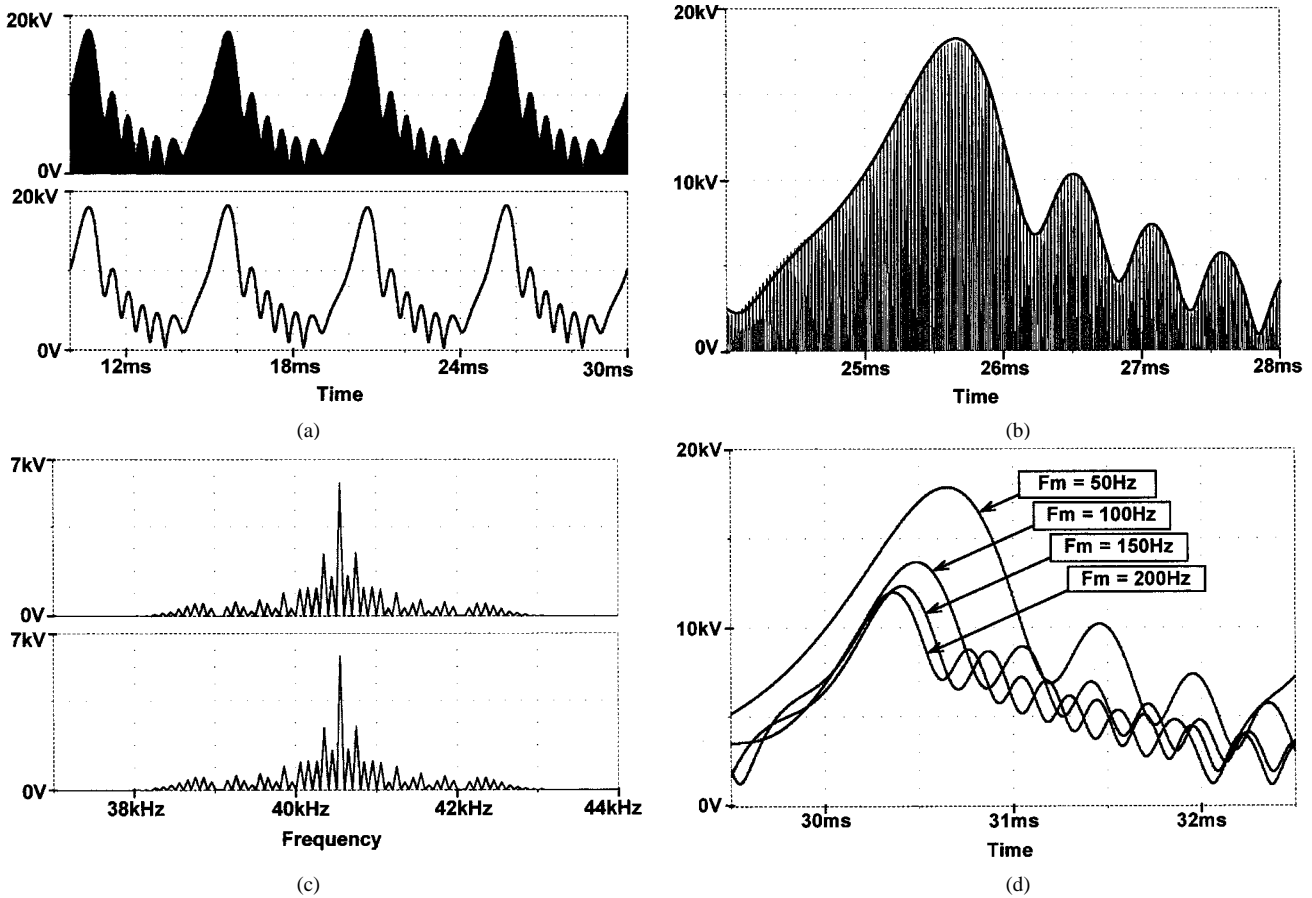
Fig. 3.   Simulation results. (a) Real component of capacitor voltage (Fig. 2) (upper trace) and envelop as obtained by envelop simulation (lower trace). (b) Zoomed portion of (a). (c) Spectrum of original circuit (upper trace) and reconstructed from envelope simulation (lower trace). (d) Envelope simulation of capacitor voltage (Fig. 2) for various modulating signals.

V. EXAMPLE

We demonstrate the technique outlined above by considering a resonant circuit (Fig. 2). It is assumed that the circuit is driven by PM modulated carrier of the form

$$v(t) = A \cos(\omega_c t + m_p \sin \omega_m t). \tag{13}$$

The circuit was transformed according to the guidelines given above and the equivalent circuits (a total of six independent circuits) were run on PSPICE. The phasor domain sources were

$$V_1 = A \cos(m_p \sin \omega_m t) \tag{14}$$

$$-V_2 = A \sin(m_p \sin \omega_m t). \tag{15}$$

For the purpose of illustration, we chose the carrier frequency $(f_c = \omega_c/2\pi)$ to be 40.55 kHz, equal to the circuit resonant frequency $1/2\pi\sqrt{LC}$. In the first run to be illustrated, the modulation parameters were: $A = 200$ V, $f_m = \omega_m/2\pi = 100$ Hz, and $m_p = 20$.

Once the time-domain simulation is done, any of the envelope signals can be displayed. For example, the envelope of the capacitor voltage (V_C) is reconstructed by the expression

$$V_C = \sqrt{(V_{1C})^2 + (V_{2C})^2} \tag{16}$$

where V_{1C} and V_{2C} are the envelope simulation results obtained for the real and imaginary parts, respectively. The degree of matching between the real signal and the results of envelope simulation [Fig. 3(a)] demonstrate the agreement that is obtained. The perfect match is illustrated in the zoomed portion [Fig. 3(b)]. Furthermore, the original spectrum of the signal and the one reconstructed from the envelope simulation results are identical [Fig. 3(c)]. The simulation time for envelope simulation was 0.5 s, as compared to 300 s with full simulation on circuit and modulated carrier. The CPU used was a 333-MHz Pentium.

Envelope simulation offers large flexibility and access to a wealth of information in a short simulation time. For example, the effect of the sweep speed on the capacitor voltage was explored by parametric simulation in which the modulating frequency was stepped from 50 to 200 Hz in 50-Hz steps while keeping the depth of modulation $m_p \cdot f_m = 4000$ constant [Fig. 3(d)]. Simulation time for this run was 10 s (on the same PC).

VI. CONCLUSION

The general and systematic approach developed here offers a simple and straightforward procedure for generating SPICE-compatible phasor equivalent circuits of any R–L–C circuit driven by any modulated signal. Although illustrated for the PM modulation case, FM and AM can be easily implemented as well. The FM case can be considered as a scaled case of PM, while the AM case is a truncated $v(t)$ signal including only a real part $V_1 = V_m \cdot (1 + m \cdot \cos \omega_m t)$. Note, however, that even in this case, the imaginary equivalent circuit

is still needed, but with $V_2 = 0$. The same methodology can be extended to any modulating function $f(x)$. It should be noted that the proposed simulation approach is not limited to sinusoidal modulation.

The systematic method for generating the auxiliary circuit is based on simple rules that can be easily mechanized to fully automate the transformation.

REFERENCES

[1] R. L. Steigerwald, "High-frequency resonant transistor DC-DC converters," *IEEE Trans. Ind. Electron.*, vol. IE-31, pp. 181–191, May 1984.
[2] B. C. Pollard and R. M. Nelms, "Using the series parallel resonant converter in capacitor charging applications," in *Proc. IEEE APEC'92*, 1992, pp. 731–37.
[3] E. Deng, "I. Negative incremental impedance of fluorescent lamp," Ph.D. dissertation, Dep. Elect. Eng., California Inst.Technol., Pasadena, CA, 1995.
[4] E. Deng and S. Cuk, "Negative incremental impedance and stability of fluorescent lamp," in *Proc. EEE APEC'97*, 1997, pp. 1050–1056.
[5] D. Sharrit, "New method of analysis of communication systems," presented at the IEEE MIT Symp. WMFA: Nonlinear CAD Workshop, June 1996.
[6] C. T. Rim and G. H. Cho, "Phasor transformation and its application to the DC/AC analyses of frequency phase-controlled series resonant converters (SRC)," *IEEE Trans. Power Electron.*, vol. 5, pp. 201–211, Apr. 1990.

Shape and Surface Measurement Technology by an Improved Shape-From-Shading Neural Algorithm

Siu-Yeung Cho and Tommy W. S. Chow

Abstract—A new approach for measuring the shape and surface of an object observed from a single camera is proposed. The proposed approach is based on using the neural networks as a parameteric representation of the three-dimensional object and the shape-from-shading problem is formulated as the minimization of an intensity error function with respect to the network weights. Experimental results demonstrate that our proposed methodology exhibits high efficiency and accuracy for measuring and inspecting the product's surface in the manufacturing industry.

Index Terms—Heuristic global learning algorithm, neural networks, shape from shading.

I. INTRODUCTION

Recently, three-dimensional (3-D) shape or surface measurement for parts, subassemblies, and finished products has become an important requirement for quality control in engineering and manufacturing. The objective of the measurement tasks is to obtain and verify the dimensions of these models (i.e., depth information) and, hence, the finished surface inspection can be performed by the 3-D geometric tolerances. In this paper, shape-from-shading (SFS) technique is employed for acquiring depth information from the two-dimensional (2-D) images. Unfortunately, conventional SFS methods [1], [2] often experience difficulties in converging toward the optimum solution. Most recently, mul-

tilayer neural networks were employed to tackle the SFS problems by learning from *a priori* knowledge [3], [4]. However, the performance of these approaches would be degraded by using ineffective gradient descent method which is of slow convergence and prone to local minima [5], especially for a complex SFS problem. Therefore, in our study, we employ a novel heuristic global learning algorithm [6], [7] for learning the neural network as object surface parameterization. This novel algorithm assures that the best possible solution can be converged within a relatively short training time. As a result, the proposed SFS algorithm is able to enhance the solving of the SFS problem in terms of the convergence speed and the avoidance of local minima. Through the numerical simulations, it is demonstrated that our proposed methodology provides an efficient, speedy, and low-cost free-form surface measurement technology.

II. NEW NEURAL-LEARNING-BASED SFS ALGORITHM

Suppose that the recovering of surface shape, represented by $z(x, y)$, from shaded images depends upon the systematic variation of image brightness with surface orientation, where z is the height field, and x and y are the 2-D pseudoplane over the domain Ω of the image plane. Assume that the object represents a Lambertain reflectance model, and that it is illuminated by a single-point source which can be computed as

$$R_{i,j}(p(x, y), q(x, y)) = \eta \mathbf{n}_{i,j} \mathbf{s}^T, \quad \forall (x, y) \in \Omega \qquad (1)$$

where i and j are the index coordinates at the corresponding pixel, η is the composite albedo, $\mathbf{s} = (s_1 \ s_2 \ s_3)$ is the illuminate source vector and

$$\mathbf{n} = \left(\frac{-p}{\sqrt{p^2 + q^2 + 1}} \ \frac{-q}{\sqrt{p^2 + q^2 + 1}} \ \frac{1}{\sqrt{p^2 + q^2 + 1}} \right)$$

is a surface normal vector, where $p = (\partial z / \partial x)$ and $q = (\partial z / \partial y)$ are the surface gradient components. Instead of solving the parameters at a finite number of points through deriving a nonlinear differential equation, the depth z can be modeled by a feedfoward neural network of which the input is a vector of $(x \ y)$ over the domain Ω and the output is the surface depth z. The number of hidden units is usually dependent on the image size, for instance, if an $N \times N$ size of the image is obtained, in our study, at least N hidden units would be used. The network weights are learned from the intensity constraints. The surface gradients and normal are able to be computed by the trained network. For simplicity, a single-hidden-layer network is used as

$$z = \sum_{g=1}^{N} v_g \sigma(w_{g1} x + w_{g2} y + \theta_g) + b_0 \qquad (2)$$

where N is the number of hidden nodes, $\sigma(x)$ is defined as a nonlinear activation function taking the form of $\sigma(x) = (1/(1 + \exp(-x)))$. $\{v_g, b_0, w_{g1}, w_{g2}, \theta_g\}$ are the network weights. Based on the above configuration, the partial derivatives of the surface gradients p and q can be defined as $p = \mathbf{m}_p \mathbf{v}$ and $q = \mathbf{m}_q \mathbf{v}$. The vector $\mathbf{v} = (v_1, v_2, \cdots, v_N, b_0)^T$ is the weights between the output and hidden layers. The vectors

$$\mathbf{m}_p = \begin{pmatrix} \sigma'\{w_{11} x + w_{12} y + \theta_1\} w_{11} \\ \vdots \\ \sigma'\{w_{N1} x + w_{N2} y + \theta_N\} w_{N1} \\ 0 \end{pmatrix}^T$$